

# Trends and periodicities in the Canadian Drought Code and their relationships with atmospheric circulation for the southern Canadian boreal forest

Martin-Philippe Girardin, Jacques Tardif, Mike D. Flannigan, B. Mike Wotton, and Yves Bergeron

**Abstract:** Trends and periodicities in summer drought severity are investigated on a network of Canadian Drought Code (CDC) monthly average indices extending from central Quebec to western Manitoba and covering the instrumental period 1913–1998. The relationship and coherency between CDC indices and ocean–atmosphere circulation patterns are also examined. Trend analyses indicate that drought severity is unchanged in eastern and central Canada. Composite analyses indicate that for most of the corridor, severe drought seasons occur with a combination of positive 500-hPa geopotential height anomalies centered over the Gulf of Alaska and over the Baffin Bay. Additional severe drought seasons develop across the corridor in the presence of positive height anomalies located over or upstream of the affected regions. According to spectral analyses, the North Atlantic and the North Pacific circulation patterns modulate the drought variability at the decadal scale. Our results lead us to conclude that climate warming and the increases in the amount and frequency of precipitation in eastern Canada during the last century had no significant impact on summer drought severity. It is unlikely that linear climate change contributed to the change in the boreal forest dynamics observed over the past 150 years.

**Résumé :** Les tendances et périodicités dans la sévérité des sécheresses estivales sont analysées sur un réseau d'indices de sécheresse (CDC) moyens mensuels couvrant le corridor Québec–Manitoba et la période déterminante 1913–1998. Les relations et les cohérences entre les indices CDC et les principaux patrons de circulation atmosphérique sont également examinées. Les résultats obtenus n'indiquent aucun changement linéaire des conditions de sécheresse estivale, ni dans l'Est ni au centre du Canada. Des analyses composites indiquent qu'à travers le corridor, des saisons de sécheresse sévère ont lieu en combinaison avec des anomalies positives de la hauteur géopotentielle à 500 hPa centrées au-dessus du Golfe de l'Alaska et au-dessus de la Baie de Baffin. Des saisons de sécheresse additionnelles ont lieu à travers le corridor avec le développement d'anomalies positives au-dessus des régions affectées. D'après nos analyses spectrales, les patrons de circulations de l'Atlantique Nord et du Pacifique Nord agissent sur la variabilité des sécheresses dans l'échelle décennale. Nos résultats nous amènent à conclure que le réchauffement climatique et les augmentations de la quantité et de la fréquence des précipitations dans l'est du Canada au cours du dernier siècle n'ont eu aucun effet important sur la sévérité des sécheresses estivales. Il est donc peu probable que le changement climatique linéaire ait contribué au changement dans la dynamique de la forêt boréale enregistré au cours des 150 dernières années.

## Introduction

Fire frequency and area burned in the southeastern Canadian boreal forest have significantly diminished since the end of the “Little Ice Age” (~1850) (Bergeron et al. 2001).

Consequently, even-aged stands composed of postfire species are decreasing in proportion and this to the benefit of uneven-aged and older stands composed of shade-tolerant species (Bergeron and Dubuc 1989). Secondary disturbances (insect outbreaks and windthrows) are also playing a greater

Received 17 March 2003. Accepted 11 August 2003. Published on the NRC Research Press Web site at <http://cjfr.nrc.ca> on 16 January 2004.

**M.-P. Girardin<sup>1,2</sup> and J. Tardif.** Centre for Forest Interdisciplinary Research (C-FIR), University of Winnipeg, 515 Avenue Portage, Winnipeg, MB R3B 2E9, Canada.

**M.D. Flannigan and B.M. Wotton.** Canadian Forest Service, 1219 Queen Street East, Sault Ste Marie, ON P6A 2E5, Canada.

**Y. Bergeron.** Groupe de recherche en écologie forestière inter-universitaire (GREFI), Université du Québec à Montréal, C.P. 8888, Succursale. Centre-Ville, Montréal, QC H3C 3P8, Canada.

<sup>1</sup>Corresponding author (e-mail: [m.girardin@uwinnipeg.ca](mailto:m.girardin@uwinnipeg.ca)).

<sup>2</sup>Present address: Department of Botany, University of Manitoba, 505 Buller Building, Winnipeg, MB R3T 2N2, Canada.

role in the establishment of the forest mosaic at the landscape level. While the forest successional pathway itself is fairly well understood (Bergeron 2000), the processes regulating succession are not well elucidated. However, paleoecological evidence suggests that climate, by affecting the fire regime, determines the boreal forest species' composition (Carcaillet et al. 2001; Bergeron et al. 2002).

Bergeron and Archambault (1993) and Bergeron et al. (2001) suggested that the reduction of area burnt in eastern Canada since the 1850s reflects a change from extreme fire condition to a moister climate (i.e., fewer extreme seasons of drought). Recent analyses of instrumental meteorological records across Canada suggested significant trends in climate (both precipitation and temperature) over the 20th century for several regions of Canada (Houghton et al. 2001). From 1950 to 1998, temperature in the northeastern Canada decreased while it increased in the south and the west (Zhang et al. 2000). As well, summer precipitation increased significantly in the northeast (Mekis and Hogg 1999). Most of this increase is attributed to an increase in the frequency of small precipitation events (Zhang et al. 2001). General circulation models' outputs (Flannigan et al. 2001) also suggested that the increase in precipitation observed in the eastern boreal forest is sufficient to overcome the effect of climate warming with respect to fire weather severity. Contrasting results were found for central Canada, suggesting an increase in dry conditions as a response to climate change (Flannigan et al. 2001).

Ocean circulation patterns can alter regional climate and disturbance regimes over North America. Nigam et al. (1999) and Barlow et al. (2001) demonstrated that North Pacific sea surface temperature (SST) variability was strongly linked to large-scale patterns of drought and stream flow in the U.S.A. Bonsal et al. (1993) and Bonsal and Lawford (1999) also reported similar findings after analysing the teleconnections between Tropical and North Pacific SSTs and summer-extended dry spells in the Canadian Prairies. While the modulation between these patterns and regional climate is not well understood, there is great interest directed towards the use of circulation patterns' information for fire-climate modelling (Flannigan and Wotton 2001).

Understanding temporal changes in fire regimes cannot be entirely based on temperature and precipitation parameters. Fire is a conjunction of various weather parameters and often the result of interactions among precipitation, temperature, humidity, solar radiation, ignition agents, and wind (Van Wagner 1987; Flannigan and Harrington 1988). The daily drought indicators accounting for precipitation, evapotranspiration, and soil moisture capacity developed as components of the Canadian Fire Weather Index system (FWI; Van Wagner 1987) offer an alternative in fire-climate analyses. These indicators, which are the Fine Fuel Moisture Code, the Duff Moisture Code, and the Drought Code (Canadian Drought Code; CDC), differ in their water-holding capacity and their drying rate.

The CDC has been used infrequently for climatic studies. In Quebec, CDC indices were used as estimates of soil moisture content to explain yearly variations within tree-ring width (Archambault and Bergeron 1992; Bergeron and Archambault 1993; Tardif and Bergeron 1997; Girardin et al. 2001). Multicentury CDC reconstructions derived from tree-

ring chronologies have also been successfully used to explain multicentury shifts in atmospheric circulation (Girardin et al. 2002; Girardin et al. In press). The CDC has five aspects that are important for this study: (i) the effect of snowmelt is accounted for in its calculation, (ii) it is an adequate indicator of moisture conditions of deep organic layers in boreal conifer stands (Van Wagner 1974), (iii) it represents conditions conducive to hydric stress in boreal tree species (Bergeron and Archambault 1993; Tardif and Bergeron 1997; Girardin et al. 2001), (iv) it is an indicator of water table depth, and (v) it represents conditions conducive to fire involving deep soil layers (Turner 1972).

In this study, we construct a network of mean monthly average instrumental CDC indices distributed along the southern Canadian boreal forest. The spatiotemporal variability within the network is analysed and linked with atmospheric circulation using 500-hPa geopotential height composite analyses. Periodicities within the network are also investigated and compared with those characterizing Northern Hemisphere ocean-atmosphere circulation indices. Finally, correlation structures between CDC indices and fire frequency and area burned are analysed to assess the potential use of the CDC indices as estimates of past fire seasons. As fire history data sets are limited in time and accuracy (Murphy et al. 2000), the development of other records that reflect past fire seasons could greatly benefit the understanding of temporal changes in the boreal forest dynamics.

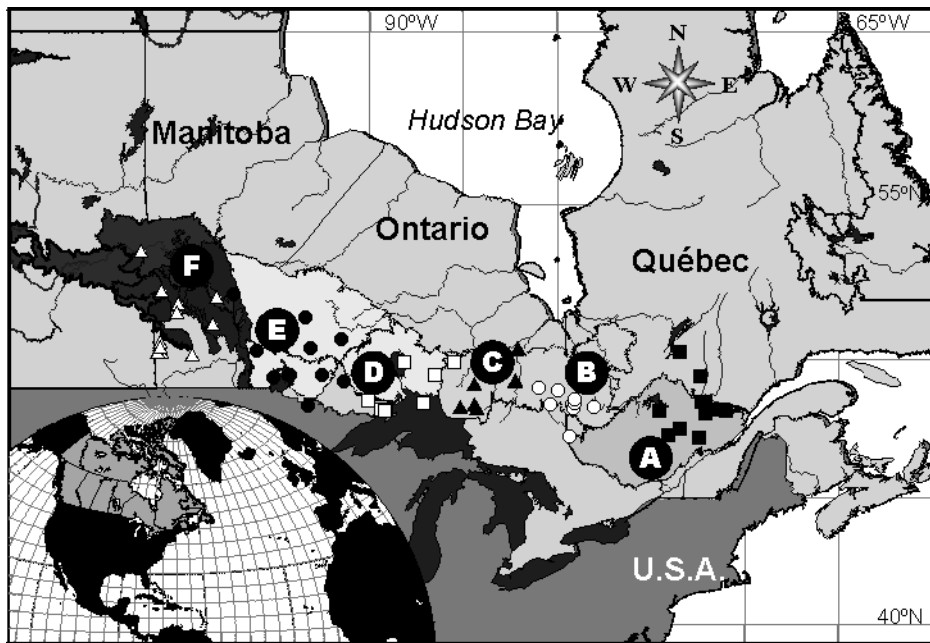
## Materials and methods

### Study area

The corridor is located on the Boreal Shield and Boreal Plains ecozones that cover most of the boreal forest from eastern Quebec to northwestern Manitoba (Fig. 1). The corridor was divided into six climatic regions (A-F; Fig. 1), with boundaries approximating actual ecoregions defined by the Ecological Stratification Working Group (1996). These climatic regions are (A) the Southern Laurentian, (B) and (C) the Abitibi Plains east and west, respectively, (D) the Lake Nipigon, (E) the Lac Seul Upland and Lake of the Woods, and (F) the Boreal Plains (Fig. 1). Merging of ecoregions in climatic regions E and F was necessary because of the lack of meteorological data required for homogenization of the CDC indices. In the Ecological Stratification Working Group's (1996) classification, the Lac Seul Upland (north) and the Lake of the Woods (south) occurs as two separate ecoregions (refer to Fig. 1). The Boreal Plains ecozone encompasses 10 separate, mostly upland ecoregions south of the Canadian Shield, stretching from north-central Alberta to southwestern Manitoba. Eastern ecoregions of the Boreal Plains ecozone were merged for the buildup of the climatic region data set: the Mid-Boreal Lowland, the Interlake Plains, the Boreal Transition, and the Mid-Boreal Uplands (Manitoba area). In contrast, the Abitibi Plains ecoregion was divided into two climatic regions (regions B and C) because of its extensive area and availability of meteorological data.

All ecoregions under study have a humid to subhumid midboreal ecoclimate (east to west corridor) marked by warm summers and cold, snowy winters according to the Ecological Stratification Working Group's (1996) regional

**Fig. 1.** Geographical locations of the 62 meteorological stations per climatic regions: A, Southern Laurentians; B, Abitibi Plains east; C, Abitibi Plains west; D, Lake Nipigon; E, Lac Seul Upland and Lake of the Woods; and F, Boreal Plains. Symbols identify the stations used in each of the climatic regions. Ecoregions, as defined by the Ecological Stratification Working Group (1996), are also drawn.



classification. In eastern climatic regions (A–D), average annual temperature ranges between 1.0 and 1.5 °C, whereas it ranges between –1.0 and 1.0 °C in regions E–F. The average summer temperature is constant across the corridor, approximately 14.0 °C. The average winter temperatures are more variable, ranging from –11.0 °C in region A to –16.0 °C in region F. The average annual precipitation ranges from 1600 mm in the east to 450 mm in the west. In this corridor, most of the annual precipitation falls between June and October (Environment Canada 2002).

### Canadian Drought Code calculation

The meteorological data used in this study were daily instrumental data of Environment Canada (2000). Meteorological stations showing the longest records (over 60 year) in the six climatic regions were selected as main stations. Other stations in a 200-km radius and with relatively long records were also selected for the calculation of homogenized monthly regional CDC indices. In some climatic regions, the number of meteorological stations and extent of the data were insufficient for the construction of homogenized data sets. In this situation, stations outside the radius were used for estimation of remaining missing values. A total of 62 meteorological stations were gathered to construct regional monthly average CDC indices. These stations are summarized in Table 1 and plotted per climatic region in Fig. 1.

Maximum daily temperature data sets were screened for the presence of missing daily values. Months (April–October) with more than 3 days of missing values were eliminated from the CDC calculation. For the remaining months, missing daily values were estimated by calculating the average of the previous and following days. For the precipitation data sets, months with at least one missing daily value were automatically eliminated from the calculation.

The CDC is sensitive to daily precipitation, such that one rainfall can significantly affect the value of the index for many days after precipitation. In contrast, a temperature estimation error of a few degrees has little impact on the calculation for the days following. Note that because the CDC calculation is on a day-to-day cumulative basis, the occurrence of a missing daily value at a station in a given year disables the CDC calculation for the rest of the year at that station.

The CDC is a slow-drying index with a time lag estimated at 52 days (Turner 1972). Its calculation was processed as proposed by Turner (1972) and Van Wagner (1987). The calculation begins with a rainfall phase (RP) value of 771 on April 1 (771 being the value normally set by fire agencies when organic layer is fully recharged). The RP, which represents the moisture equivalent after rain (expressed in percentage of dry soil), is otherwise calculated from

$$[1] \quad RP = [800/\exp(\text{CDC}_{d-1}/400)] + 3.937ER$$

where  $\text{CDC}_{d-1}$  represents the drought value of the previous day. RP can range from 0 to 800, with 800 being saturation in water and 0 being the driest condition normally encountered. RP never exceeds 800. ER (effective rainfall) is equivalent to the amount of rainfall available for storage after interception by the canopy (the constant 3.937 was introduced by Van Wagner 1987 to adapt ER to the metric system). The constant 400 represents the maximum water-holding capacity of the soil, which amounts to approximately 400% of water per units of mass. The water-holding capacity of the CDC layer is 100 mm (or 4.0 in.) for a layer with a bulk density of about 25 kg/m<sup>2</sup>. Excess water is considered as residual rainfall and is not accounted for by the CDC (see Appendix A).

**Table 1.** Meteorological stations used in the calculation of the mean monthly average Canadian Drought Code (CDC) indices.

Station	Code	Longitude	Latitude	Elevation	Period
<b>A. Southern Laurentian</b>					
Normandin	7065640	72°32'W	48°51'N	137	1937–1992
Roberval airport	7066685	72°16'W	48°31'N	179	1958–1998
Roberval	7066688	72°14'W	48°32'N	102	1888–1966
Mistassini	7064998	72°12'W	48°51'N	122	1964–1994
Albanel	7060080	72°27'W	48°53'N	152	1923–1990
Bagotville	7060400	71°00'W	48°20'N	159	1943–1998
Lac Bouchette	7063560	72°10'W	48°13'N	358	1951–1998
Chicoutimi	7061441	71°50'W	48°25'N	175	1881–1979
Hemon	7063090	72°36'W	49°40'N	183	1966–1998
Kenogamie	7063400	71°15'W	48°25'N	116	1924–1964
Barrage à Lac Kempt	7070448	74°11'W	47°33'N	421	1913–1963
Barrage Gouin	7070454	74°06'W	48°21'N	404	1914–1979
La Tuque	7074240	72°47'W	47°24'N	152	1915–1998
Manouan Sanmaur	7074600	73°48'W	47°54'N	357	1919–1972
Mistassini Post	7095000	73°53'W	50°25'N	380	1899–1980
<b>B. Abitibi Plains east</b>					
Abitibi Post	7090050	79°22'W	48°43'N	259	1898–1935
Amos	7090120	78°07'W	48°34'N	259	1915–1997
Duparquet	709BBDH	79°16'W	48°31'N	290	1983–1993
La Sarre	7094120	79°12'W	48°48'N	244	1952–1998
Val Saint-Gilles	70986RN	79°07'W	48°59'N	290	1973–1998
Cochrane	6071712	81°02'W	49°04'N	275	1912–1991
Iroquois Falls	6073810	80°40'W	48°45'N	259	1913–1997
Kirkland Lake	6074209	80°00'W	48°90'N	324	1951–1996
Haileysbury	6073138	79°38'W	47°27'N	189	1895–1922
<b>C. Abitibi Plains west</b>					
Franz	6052563	84°25'W	48°28'N	373	1918–1949
Hornepayne	6053570	84°46'W	49°12'N	329	1920–1989
Steep Hill Falls	6058010	84°48'W	48°40'N	335	1920–1938
White River	6059475	85°17'W	48°36'N	379	1889–1975
Kapuskasing A	6073960	82°28'W	49°25'N	227	1919–1998
Kapuskasing	6073975	82°26'W	49°27'N	218	1937–1998
Smokey Falls	6077845	82°10'W	50°40'N	183	1934–1996
<b>D. Lake Nipigon</b>					
Cameron Falls	6041109	88°21'W	49°90'N	229	1925–1997
Geraldton A	6042716	86°56'W	49°47'N	349	1981–1998
Kakabeka Falls	6043930	89°37'W	48°24'N	278	1910–1976
Port Arthur	6046588	89°13'W	48°26'N	195	1878–1941
Schreiber	6047624	87°16'W	48°49'N	302	1910–1975
Thunder Bay A	6048261	89°20'W	48°22'N	199	1942–1993
Manitouwadge	6044903	85°48'W	49°90'N	332	1956–1994
Savanne	6047615	90°12'W	48°58'N	459	1892–1946
<b>E. Lac Seul Upland and Lake of the Woods</b>					
Dryden	6032117	92°50'W	49°47'N	372	1914–1997
Ignace	6033690	91°39'W	49°25'N	447	1914–1970
Kenora	6034070	94°32'W	49°48'N	336	1900–1938
Kenora A	6034075	94°22'W	49°47'N	410	1939–1998
Sioux Lookout	6037775	91°54'W	50°70'N	390	1939–1998
Fort France	6022475	93°25'W	48°37'N	343	1892–1995
Earl Falls	6012198	93°13'W	50°38'N	361	1930–1996
Red Lake A	6016975	93°48'W	51°40'N	386	1939–1998
Channel Island	5030556	97°23'W	52°18'N	216	1890–1904
Great Falls	5031200	96°00'W	50°28'N	249	1923–1996
Indian Bay	5031320	95°12'W	49°37'N	327	1915–1998

**Table 1** (concluded).

Station	Code	Longitude	Latitude	Elevation	Period
<b>F. Boreal Plains*</b>					
Dauphin	5040675	100°20'W	51°90'N	292	1890–1941
Swan River	5042800	101°13'W	52°30'N	347	1910–1998
Dauphin A	5040680	100°30'W	51°60'N	305	1943–1998
Gilbert Plains	5040985	100°28'W	51°60'N	404	1959–1998
Moosehorn	5041800	98°37'W	51°18'N	250	1910–1963
Russell Barnardo	5042522	101°20'W	50°59'N	558	1896–1906
Ashern	5040120	98°22'W	52°08'N	263	1967–1989
Russell	5012520	101°17'W	50°46'N	567	1884–1990
Cumberland House	4071960	102°18'W	53°58'N	271	1937–1964
Minnedosa	5011760	99°50'W	50°16'N	521	1881–1998
Fort Ellice	5010977	101°14'W	50°25'N	NA	1890–1894
Birtle	5010240	101°30'W	50°26'N	522	1917–1995

**Note:** Elevation (m) is above sea level. NA, not available.

\*The Boreal Plains regional data set was created using the first nine weather stations listed. Remaining missing values within the regional data set were estimated using three other stations (i.e., Minnedosa, Fort Ellice, and Birtle) located southward.

ER is calculated from

$$[2] \quad ER = 0.83P - 1.27$$

where  $P$  represents the daily value of precipitation over 2.80 mm (intercepted rainfall). ER is not calculated unless precipitation exceeds 2.80 mm. The values of 0.83 and 1.27 mm are empirical constants representing canopy interception.

Current drought ( $D$ ) is calculated using the RP value of eq. 1 and the following equation:

$$[3] \quad D = 400 \ln(800/RP)$$

The calculation of the potential evapotranspiration (PET) (the daily dry-weather additive) is given by

$$[4] \quad PET = 0.36T + L$$

$T$  represents the maximum daily temperature value (°C), and  $L$  represents a seasonal day length adjustment. From April to October, the values of  $L$  are 0.9, 3.8, 5.8, 6.4, 5.0, 2.4, and 0.4, respectively (Van Wagner 1987). The PET calculation follows Thornthwaite and Mather (1955). The maximum daily temperature was not adjusted to the noon local standard time, as it is normally done in the FWI system (Turner 1972; Van Wagner 1987). The value of 0.36 is the average relationship between maximum temperature and PET (Turner 1972).

The CDC is calculated from

$$[5] \quad CDC = D + 0.5PET$$

Because the scale length of the CDC is one-half that of the original scale used by Turner (1972), the value of PET is halved (see Van Wagner 1987). A CDC rating of 200 is high, and 300 or more is extreme, indicating that fire will involve deep subsurface and heavy fuels (Van Wagner 1987).

Calculation of the RP (eq. 1) for April 2 is realised using the CDC value (eq. 5) and the ER (eq. 2) of April 1. Using the RP result from April 2, eqs. 3 and 4 are processed for calculation of the April 2 CDC value. This procedure is repeated until October 31. Calculation of next year's CDC is started at April 1 with an RP value of 771. In our corridor, the probability that a current drought persists the following

year as a result of insufficient winter precipitation is minimal (overwintering effect, Van Wagner 1987). Thus, no adjustment was made to the CDC calculation.

The effect of snowmelt on the starting value of the CDC was simulated accordingly with Turner's (1972) criteria. The snowmelt date is assumed to be the time at which the forest floor is saturated with water (usually occurs in May) and closely corresponds with a decreasing RP of five units a day for 3 days. The procedure that accounts for snowmelt was made as follows. For a given year, the CDC was calculated using eqs. 1–5 with an RP starting value of 771 set at April 1 (refer to eq. 1). Then, the output of the RP calculation was monitored, beginning in April. The initial value of 771 set at April 1 was delayed to the third consecutive day of decreasing RP of five units. The CDC was recalculated for the whole year based on that new starting date.

### Regional monthly average indices

Monthly average CDC data files were created for each station. Because of changes in measuring instruments and of station relocations through time, nonhomogeneity in the monthly indices may be observed among nearby meteorological stations (Mekis and Hogg 1999; Vincent and Gullet 1999). A test of homogeneity for identification of nonhomogeneous stations was performed between each pair of climate data sets according to the Holmes' (1999) procedure. The Mann–Kendall statistical test for randomness was performed on each paired data set. A pass–fail test was made at the 95% critical limit. All stations failing the test were rejected, unless the anomalies could be corrected. The regional monthly averages of CDC indices were calculated using program MET (Holmes 1999). In this procedure, the average and standard deviation were calculated for each month at each station. The departure for each month and year was then calculated and averaged across stations to produce mean regional average departures for each month and year. Files of regional mean monthly average CDC indices per climatic region were then produced and used in further analyses.

Gaps in CDC indices within single meteorological stations (Table 1) were also filled using Holmes' (1999) proce-

ture. Missing monthly values were estimated by calculating the value with a departure from the mean for the month at that station equal to the average departure of the other stations for that month and year. The standard deviation for the month at that station was multiplied by the regional average departure for the month and year, and the mean value for the month at the station was added. New files with estimated data were produced.<sup>3</sup> These data sets were developed for distribution in the scientific community and are not used throughout this paper.

### Trends, periodicities, and spatial correlation

The presence of a linear trend in the regional mean monthly average CDC was determined using linear regression analyses for the period 1913–1998. This period was chosen so that all analyses could be performed on the same sample size. Autocorrelation analyses, monthly lagged correlation analyses, and Durbin–Watson tests were also performed on the indices. The presence of autocorrelation was tested, as autocorrelation reduces the effective number of independent observations and thus reduces the degrees of freedom used to determine the confidence in estimates of correlation coefficients (Legendre and Legendre 1998).

Continuous wavelet transform (CWT) spectrums were created for identification of nonstationary periodicities within CDC indices (Lau and Weng 1995). CWTs were processed from a nonorthogonal Morlet 6 wavelet basis, a Gaussian-windowed complex sinusoid (Torrence and Compo 1998; Program AutoSignal (version 1.5), AISN Software 1999). The wavelet basis was selected so that the time–space domain is maximized in length over the spectral–space domain (Torrence and Compo 1998). All time series were normalized before processing the CWT spectrums. Zero padding was used to eliminate the wraparound effect (see Torrence and Compo 1998).

Spatial patterns among the monthly average CDC indices were examined using S-mode principal component (PC) analyses performed on correlation matrices (Yarnal 1993; Legendre and Legendre 1998; ter Braak and Smlauer 1998; Barry and Carleton 2001). In this procedure, the monthly CDC data sets were transformed into new sets of monthly composite variables. The amount of variability is described using the same number of variables, but with the first principal component (PCI) accounting for the maximum possible proportion of the variance. Succeeding PCs, in turn, account for as much of the residual variance as possible. Eigenvectors, or the loading of each CDC indices on each component, gives the spatial representation of the PCs.

### Ocean–atmosphere circulations

Composite maps performed on 500-hPa geopotential heights, which approximate the actual height above sea level of the 500-hPa pressure surface, were created with the aid of the National Oceanic and Atmospheric Administration – Cooperative Institute for Research in Environmental Sciences (NOAA–CIRES) Climate Diagnostics Center, Boulder, Colo. (Kalnay et al. 1996; [www.cdc.noaa.gov](http://www.cdc.noaa.gov)). The 500-hPa grid has a global spatial coverage of 2.5° latitude × 2.5° lon-

gitude with 144 × 73 points and a temporal coverage of 1948 to present, with output every 6 h. Daily 500-hPa heights were averaged by months for each grid point. 500-hPa anomalies (expressed in m) were calculated for each calendar month and at each grid point based on the period 1968–1996. Composites were created for seasons of 10 severe (10 highest CDC values) and 10 low (10 lowest CDC values) drought conditions. These seasons represent the upper and lower 20% of the sample population.

Coherency between CDC indices and atmospheric circulation indices at various time and period scales were identified using the cross product of the CWTs (Torrence and Compo 1998; Torrence and Webster 1998). For comparison, periodicities showing coherency were reconstructed with the use of spectral components isolated in the time–frequency domain. The atmospheric circulation patterns under study are the North Atlantic Oscillation (NAO; Hurrell 1995), the Pacific Decadal Oscillation (PDO; Mantua et al. 1997), and the Southern Oscillation (SO; Ropelewski and Jones 1987).

The NAO is defined as the north–south sea level pressure dipolar pattern, with one of the centres located over Ponta Delgada, Azores, and the other one approximately over Iceland. A positive NAO value indicates strong midlatitude westerlies and is characterized by an intense Iceland Low with a strong Azores Ridge to its south. A negative NAO value indicates that the signs of these anomaly cells are reversed. Over the subtropical Pacific, the SO reflects a difference in sea level pressures between Tahiti and Darwin. A positive SO is an indication that sea level pressure is higher than normal in the Southeast Pacific. Finally, the PDO consists of the leading PC of the North Pacific monthly SST poleward of 20°N. A negative PDO value is an indication that SSTs are anomalously warm in the interior North Pacific and cool along the Pacific Coast.

### Drought and fire history

The CDC indices were correlated with forest area burned (surface burned per year per climatic region) and forest fire frequency (number of fires per year per climatic region) using PC analyses. Fire statistics were introduced as supplementary variables and do not affect the formation of the PCs; the PCs are the linear combinations of the mean monthly average CDC indices. Forest fire statistics were compiled for each climatic region using the forest fire data set of Stocks et al. (2003; period 1959–1998). The forest fire data set only includes fires greater than 200 ha in final size. This represents only a few percent of all fires, but accounts for most of the area burned (more than 97%, Stocks et al. 2003). The forest fire – CDC comparison is made without consideration for the time (i.e., month) and cause of fire ignition. According to Skinner et al. (1999), 84% of all total area burned in Canada occurs during June, July, and August.

## Results

### Monthly trends

Across the corridor under study, the month during which maximum drought severity is attained is August (Fig. 2).

<sup>3</sup>Supplementary data for this article are available on the Web site or may be purchased from the Depository of Unpublished Data, Document Delivery, CISTI, National Research Council Canada, Ottawa, ON K1A 0S2, Canada. DUD 3541. For more information on obtaining material refer to [http://www.nrc.ca/cisti/irm/unpub\\_e.shtml](http://www.nrc.ca/cisti/irm/unpub_e.shtml).

**Fig. 2.** Regional mean monthly average Canadian Drought Code (CDC) indices (left column). The period prior 1913 in (a) and (e) contains uncertainties and missing values attributed to the number of station replicates for mean of comparison. The right column shows the average (with error bars) of the mean monthly values (April–October) for the period 1913–1998. A different shade is given for each month (refer to right column for month identification). Note the different y axis scale for (e) and (f).

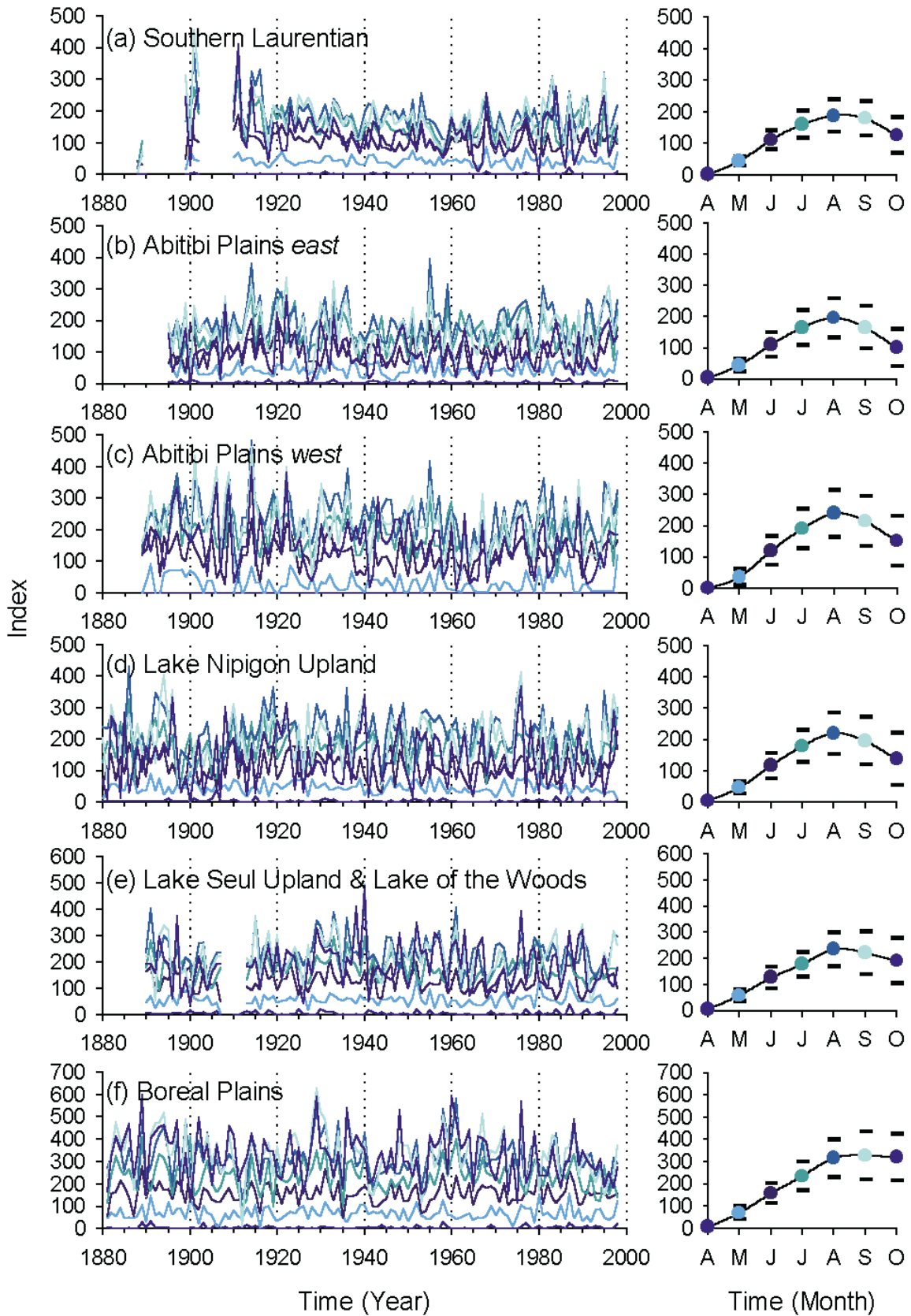
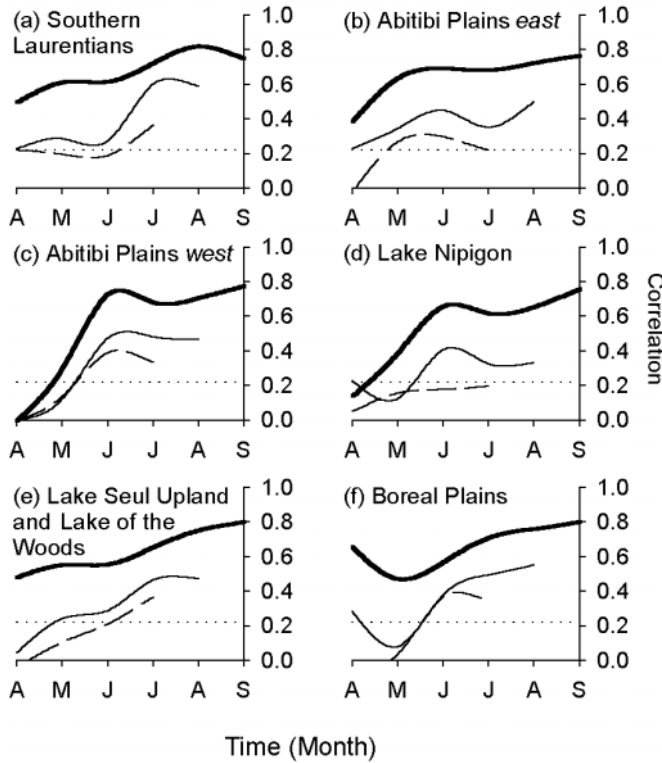


**Fig. 3.** Monthly lagged Pearson's correlation coefficients. Analyses were conducted for the period 1913–1998. The thick line shows the correlation coefficient between a month and the following one (e.g., April vs. May). The thin line shows the correlation coefficient with the second following month (e.g., April vs. June). The dashed line shows the correlation coefficient with the third following month. The significance level at  $p < 0.05$  is given by the dotted line.



Drought severity decreases in September in climatic regions A, B, C, D, and E. In region F, it remains stable from August to October. Monthly lagged correlation analyses (Fig. 3) further suggest significant persistence in the monthly CDC indices (e.g., droughts that occur in June also occur in July ( $p < 0.001$ ), August ( $p < 0.05$ ), and September ( $p < 0.05$ )).

The CDC indices shown in Fig. 2 indicate that episodes of extreme drought conditions (values greater than 300) constantly occur within region F. This contrasts with the eastern regions, which experienced a marked decrease in the frequency of extreme drought conditions in the early 1900s. Linear regression analyses performed on the monthly average CDC indices (Table 2), however, indicate no general trend toward a decrease or increase in drought severity across the corridor (only 1 significant result out of 42 tests). None of the CDC indices contain autocorrelation (Table 2).

**Analyses of periodicities**

For simplification, nonstationary periodic signals were examined within the July mean monthly average CDC indices only. The high monthly autocorrelation (see Fig. 3) justified the assumption that the variance within the month of July is also representative of June and August. Figure 4 indicates that all climatic regions display high power in the frequency band 0.20–0.50 cycles/year (2–5 years/cycle). Power is

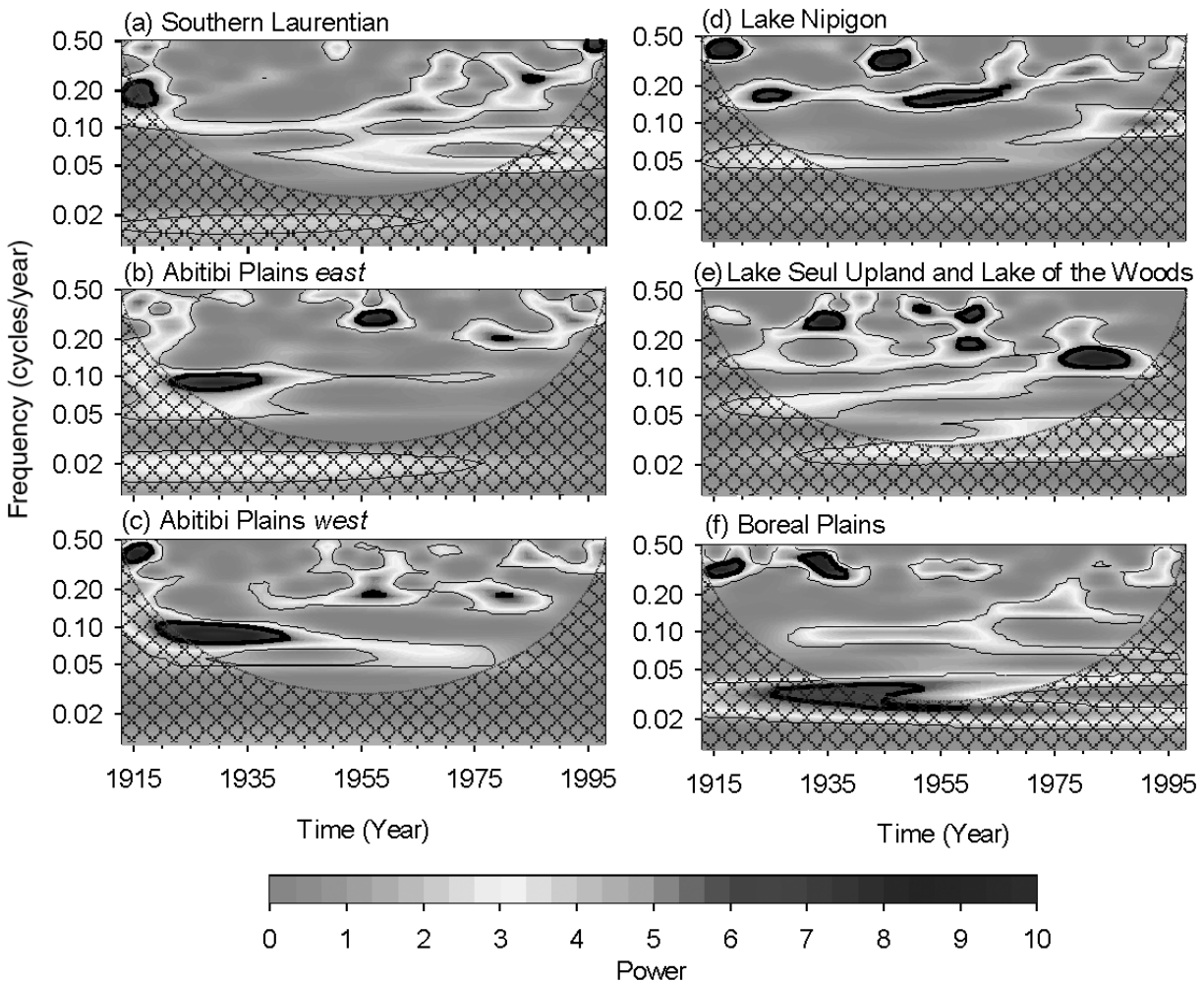
**Table 2.** Analyses of Canadian Drought Code (CDC) monthly trends, period 1913–1998.

Month	R	Slope	p	D–W	Auto-R
<b>A. Southern Laurentian</b>					
April	0.07	0.01	0.51	1.88	0.02
May	0.01	0.00	0.95	2.17	–0.10
June	0.06	–0.07	0.58	2.06	–0.03
July	0.16	–0.28	0.13	2.00	–0.02
August	0.18	–0.37	0.09	1.83	0.07
September	0.12	–0.25	0.29	1.79	0.10
October	0.00	–0.23	0.35	1.91	0.04
<b>B. Abitibi Plains east</b>					
April	0.15	0.03	0.17	1.86	0.07
May	0.05	0.04	0.62	2.33	–0.21
June	0.05	–0.08	0.64	1.90	0.03
July	0.10	–0.22	0.37	2.17	–0.10
August	0.09	–0.22	0.43	1.77	0.10
September	0.07	–0.18	0.54	1.79	0.10
October	0.00	–0.25	0.34	1.93	0.03
<b>C. Abitibi Plains west</b>					
April	0.03	0.00	0.78	1.84	–0.01
May	0.07	0.07	0.51	2.06	–0.08
June	0.02	0.03	0.87	1.67	0.16
July	0.12	–0.31	0.26	2.08	–0.06
August	0.19	–0.59	0.07	2.02	–0.02
September	0.17	–0.55	0.12	2.00	0.01
October	0.21	–0.67	0.05*	2.14	–0.07
<b>D. Lake Nipigon Upland</b>					
April	0.04	0.01	0.71	2.24	–0.12
May	0.16	–0.12	0.15	2.20	–0.05
June	0.02	0.03	0.86	1.93	–0.01
July	0.09	–0.17	0.44	2.06	–0.07
August	0.12	–0.32	0.27	2.09	–0.05
September	0.01	–0.04	0.91	2.11	–0.07
October	0.08	–0.28	0.44	2.15	–0.09
<b>E. Lac Seul Upland and Lake of the Woods</b>					
April	0.02	0.01	0.83	2.13	–0.10
May	0.01	0.01	0.92	2.13	–0.07
June	0.05	–0.09	0.63	1.83	0.08
July	0.19	–0.36	0.08	1.80	0.09
August	0.01	–0.37	0.20	1.90	0.04
September	0.12	–0.38	0.29	2.09	–0.05
October	0.13	–0.44	0.24	2.05	–0.03
<b>F. Boreal Plains</b>					
April	0.07	0.02	0.52	2.05	–0.08
May	0.03	–0.03	0.80	2.30	–0.18
June	0.00	–0.01	0.98	2.18	–0.09
July	0.08	–0.21	0.46	1.97	–0.01
August	0.10	–0.33	0.38	1.85	0.06
September	0.15	–0.66	0.16	1.81	0.09
October	0.15	–0.62	0.17	2.15	–0.08

**Note:** R, multiple correlation of the linear trend model; p, analyses of variance significance level (hypothesis that the slope of the regression line is zero is rejected when  $p < 0.05$ ); D–W, Dublin–Watson statistic (significant at  $p < 0.05$  if  $1.67 > d > 2.33$ ); Auto-R, first-order autocorrelation (significant at  $p < 0.05$  if  $-0.22 > r > 0.22$ ).

\*Significant at  $p < 0.05$ .

**Fig. 4.** Continuous wavelet transform (CWT) spectrums of Canadian Drought Code (CDC) indices for July per climatic region. Analyses were conducted for the period 1913–1998. The period (years/cycle) of each peak is given by the conversion  $1/\text{frequency}$ . The variance (in normalized units) is scaled from 0 to 10, where black area indicates large power. The thick contour line delineates the 5% significance level for white noise. The crosshatched region delineates the cone of influence (area of decreased variance resulting from a discontinuity introduced at the end of the data stream; Torrence and Compo 1998).



higher in climatic regions D, E, and F around 1915, 1935, 1945, and 1955. A periodicity of 0.10–0.20 cycles/year (5–10 years/cycle) is observed in climatic regions D and E. Maximum magnitude was attained during 1915–1940 and 1945–1965 in region D and during 1975–1990 in region E. The strongest periodicity, in the range of 0.05–0.10 cycles/year (10–20 years/cycle), is observed in climatic regions B and C. The lowest periodicity, in the frequency band 0.02–0.05 cycles/year (20–50 years/cycle), is observed in region F. Caution should be taken in the interpretation of this signal, as it is located within the cone of influence.

#### Spatial distribution of the variance

The identification of basic climatological patterns within the corridor was performed by decomposing the indices into six uncorrelated PCs. Scree plots (Yarnal 1993; results not shown) indicated that PCs I, II, and III were to be used in the interpretation. An exception is found for April, as only two PCs were necessary to describe most of the variation.

Correlation structures (eigenvectors) are shown as correlation maps in Fig. 5. There is a distinctive reduction in the

amount of explained variance by the first eigenvector from April to July (first column). The percentage of explained variance notably decreases by 24.1% to the benefit of eigenvector II, for which the explained variance increases by more than 10% (second column). The correlation maps suggest that prior to July, only one pattern (PCI) dominates the corridor. By July, the partitioning of the variance along higher eigenvectors (Figs. 5j and 5k) is suggestive of additional patterns. One pattern (explained variance by eigenvector II) appears over the western climatic regions (Fig. 5, second column), with a variance uncorrelated with the eastern sector. This pattern slowly retreats from the western sector around August. Another pattern, for which the variance is explained by eigenvector III, is seen in central Quebec (Fig. 5, third column). This pattern remains present for most of the drought season, with some monthly variations (Figs. 5k and 5n).

#### 500 geopotential height anomalies

Upper atmospheric circulation anomalies associated with low and severe drought seasons for the July PCI, PCII, and

**Fig. 5.** First, second, and third eigenvectors of the regional monthly average Canadian Drought Code (CDC) indices for April–October. The shadings indicate the correlation coefficients between the regional indices and the corresponding principal component. Correlation are significant at  $p < 0.01$  when  $-0.28 > r > 0.28$ . For each map, the percentage of explained variance is indicated.

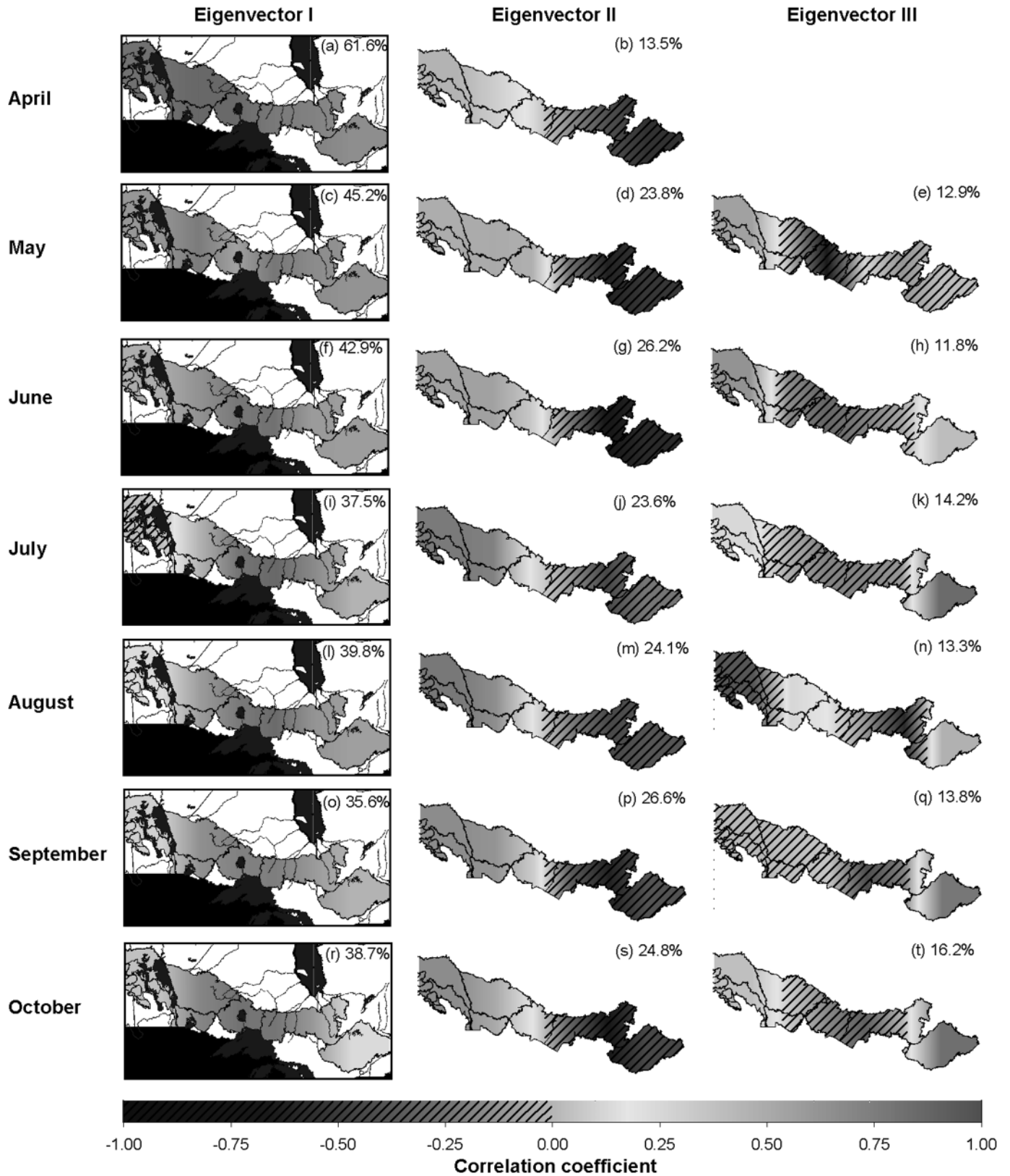
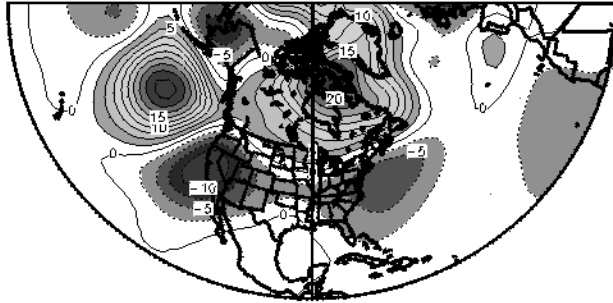


**Fig. 6.** The 500-hPa geopotential height anomaly composites (in metres) for 10 seasons of severe and 10 seasons of low drought conditions for July: (a, b) principal component (PC) I, (c, d) PCII, and (e, f) PCIII (period 1948–1998). The May–July season was used in the calculation of the height data. Years used in the composites are listed above each map (in order of increasing drought severity).

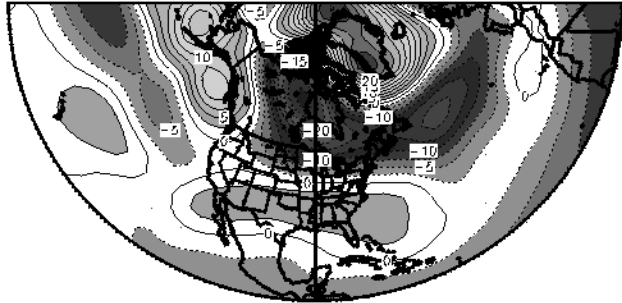
(a) PCI - severe

1983, 1948, 1987, 1975, 1967, 1960, 1980, 1976, 1998, 1955



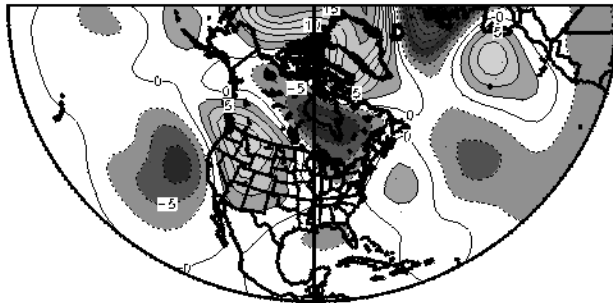
(b) PCI - low

1950, 1984, 1990, 1968, 1964, 1958, 1978, 1997, 1952, 1957



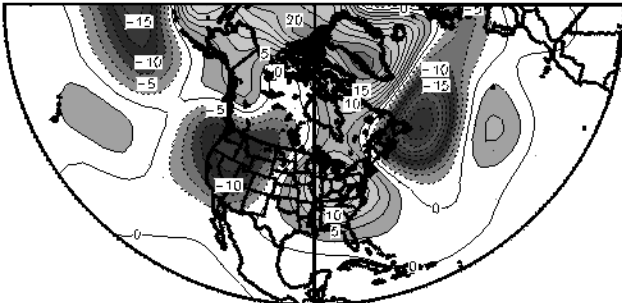
(c) PCII - severe

1970, 1957, 1987, 1972, 1958, 1974, 1980, 1960, 1979, 1961



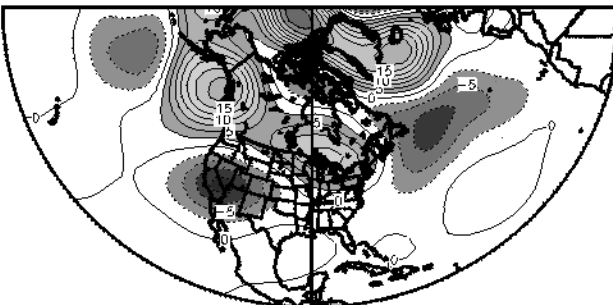
(d) PCII - low

1991, 1977, 1953, 1994, 1993, 1959, 1983, 1965, 1993, 1968



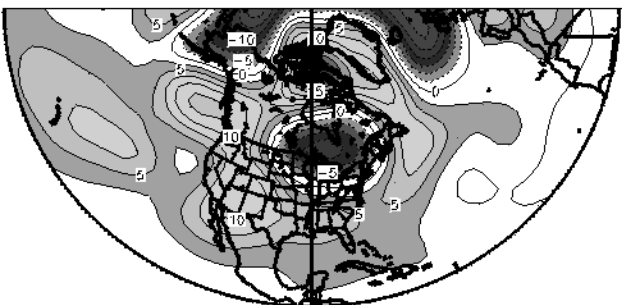
(e) PCIII - severe

1988, 1971, 1989, 1982, 1967, 1987, 1951, 1991, 1995, 1968



(f) PCIII - low

1996, 1998, 1959, 1981, 1994, 1970, 1985, 1973, 1958, 1948



PCIII were investigated using composite analyses (refers to Fig. 5 for partitioning of the variance). Figure 6a indicates that on average, severe drought seasons in Ontario occurred with the development of positive geopotential height anomalies (ridges), with centres over the Baffin Bay (24 m) and the Gulf of Alaska (20 m). Negative height anomalies (troughs) accompany this over the east and west coasts of the U.S.A. During low severity drought seasons, the positive height anomaly over Baffin Bay is split and displaced over Greenland, allowing a strong zonal flow (-24 m) to penetrate from northern Manitoba toward central Quebec (Fig. 6b). This flow further penetrates into the North Atlantic basin between 30°N and 50°N (-16 m). The positive

height anomaly over the Gulf of Alaska is displaced above the Bering Sea.

Drought seasons in southwestern Manitoba can also develop with the occurrence of positive height anomalies, with centres over the northwestern U.S.A. (10 m), the Norwegian Sea (16 m), and the Arctic (16 m) (Fig. 6c). The flow is displaced northward over northern Manitoba and Ontario (-10 m), well penetrating in Quebec. During low drought seasons (Fig. 6d), the northwestern U.S.A. positive height anomaly is replaced by a negative anomaly (-12 m), which penetrates inward Manitoba, while a positive anomaly (14 m) develops in the eastern U.S.A. In addition, the Norwegian Sea positive height anomaly is displaced over the

Baffin Bay, while the positive anomaly over the Arctic weakens. This configuration of positive and negative height anomalies that reverses from severe drought to low drought seasons would explain much of the negative correlation observed in PCII between eastern and central Canada (refer to Fig. 5j).

Drought seasons in central Quebec can also coincide with the occurrence of a positive height anomaly (10 m) centred over the Great Lakes (Fig. 6e). This anomaly displaces the flow over northeastern Quebec. This is also accompanied by positive height anomalies over the northeast of Gulf of Alaska (20 m), the Arctic (25 m), and Iceland (20 m). During low drought seasons (Fig. 6f), a negative height anomaly replaces the positive anomaly located over the Great Lakes. This negative height anomaly is surrounded by a positive anomaly with split centres over the Baffin Bay and over the western coast.

### Atmosphere–ocean circulation indices

The origin of the variance within the July PCI, PCII, and PCIII was also examined using atmospheric circulation indices (NAO, PDO, and SO). First, the Mann–Whitney statistical test was performed to test for differences in mean among samples of NAO, PDO, and SO indices at the time of the 10 highest (severe droughts) and the 10 lowest CDC values (period 1913–1998). For the analyses of PCI, the test indicated statistically significant differences at  $p < 0.01$  between the means of NAO during severe and low drought seasons. On average, severe drought seasons correspond with positive NAO values (mean of 0.67), while low drought seasons correspond with negative NAO values (mean of  $-0.75$ ). A similar relationship at  $p < 0.05$  was seen in PCIII. Severe drought seasons occur in conjunction with decreased NAO values (mean of  $-1.12$  for severe vs. 0.03 for low). Tests performed on PCII and on SO and PDO indices were nonsignificant.

Coherencies between CDC indices and atmospheric circulation pattern indices in time and period scales were investigated by crossing CWTs of July PCI, PCII, and PCIII with CWTs of the atmospheric circulation indices (May–July seasonal average). The NAO demonstrates the strongest coherency with PCI (with peaks similar to Figs. 4b, 4c) and to some extent with PCII and PCIII (Figs. 7a–7c). The coherency shifts from one band to another, being at 0.05–0.20 cycles/year in the first half of the century and around 0.50–0.10 cycles/year in the middle (Fig. 7a). Reconstruction of the 0.05–0.20 cycles/year (5–20 years/cycle) waveform (Fig. 8a) shows that this NAO modulation would explain much of the variance within PCI from 1913 to 1962 ( $R^2$  of 17.3%,  $p < 0.01$ ). The relationship is no longer significant for the period post-1962 (decoupling between the NAO waveform and PCI beginning in the 1970s).

The PDO is demonstrating coherency with the PCs, mainly in the low frequency band (0.02–0.05 cycles/year) (Figs. 7d–7f). Reconstruction of the 20–25 years/cycle waveforms, however, demonstrates that this coherency contrasts among climatic regions. In PCII, this coherency is in phase and positive (Fig. 8b). In PCIII, the coherency is in phase, but negative (Fig. 8c). The PDO modulation would explain much of the low frequencies seen in Figs. 4e and 4f. As for the SO, peaks unique to the pattern are present ca.

1910–1920 (Fig. 7i) and ca. 1970–1990 (Fig. 7h) in the band 0.13–0.30 cycles/year. Other peaks in the band 0.20–0.50 cycles/year are seen in the 1910s, the 1940s–1950s, and the 1990s.

### Drought severity and fire history

Correlation maps presented in Fig. 9 indicate good agreement between area burned and drought severity. The drought severity variance associated with the first eigenvector (Fig. 9a) is significantly correlated with the seasonal area burned in climatic region D. The drought severity variance associated with the second eigenvector (Fig. 9b) is significantly correlated with area burned in climatic region F. The drought severity variance associated with the third eigenvector (Fig. 9c) correlates significantly with area burned in regions A and B (both correlations are of 0.31). The analysis performed on fire frequency indicates very similar tendencies (except for the second eigenvector for which results were nonsignificant). July CDC indices are representative of the overall variance in seasonal area burned and fire frequency (based on analyses of fires with final area greater than 200 ha; period 1959–1998).

## Discussion

### Trends, periodicities, and variance

Linear regressions analyses performed on CDC indices indicate that 20th century linear increases in summer temperature and in the amount and frequency of precipitation (Mekis and Hogg 1999; Zhang et al. 2000, 2001) have no significant impact on the moisture balance of the deep organic layer. However, other components of the boreal forest's water balance may be affected by climate change (e.g., more or less rainfall could be intercepted by the canopy, the fine fuels, and the duff layer). Critical investigation of the FWI and each of its compartments should thus be performed. Studies should focus on average, minimum, and maximum monthly and seasonal values and on length of the seasons.

The absence of trends within the CDC indices suggests that factors other than a linear change in climate contributed to the shift in the eastern Canada's boreal forest dynamics over the past 150 years (Bergeron 2000; Bergeron et al. 2001). This interpretation assumes that the processes regulating the fire regime are stationary in time (i.e., they remain unchanged from one period to another). Our results thus give credence to Bergeron and Archambault (1993) and Lefort et al. (2003), who suggested that an increase in the fire cycle length (i.e., length of time required to burn an area equal in size to a specified area) since the 1850s in the eastern Canadian boreal forest is a response to a decrease in the frequency of events conducive to extreme fire conditions. These extreme drought events would be similar to those experienced during the 1910s and 1920s (Figs. 2a–2c), the period of largest area burned over the past 150 years in the Abitibi Plains (Bergeron et al. 2001). The 1850s phenomena could be attributed to a shift in atmospheric circulation and its drivers (PDO and NAO variability; Girardin et al. 2002; Girardin et al. In press), possibly a decrease in the frequency of occurrence of the 500-hPa geopotential height configuration seen in Fig. 6a.

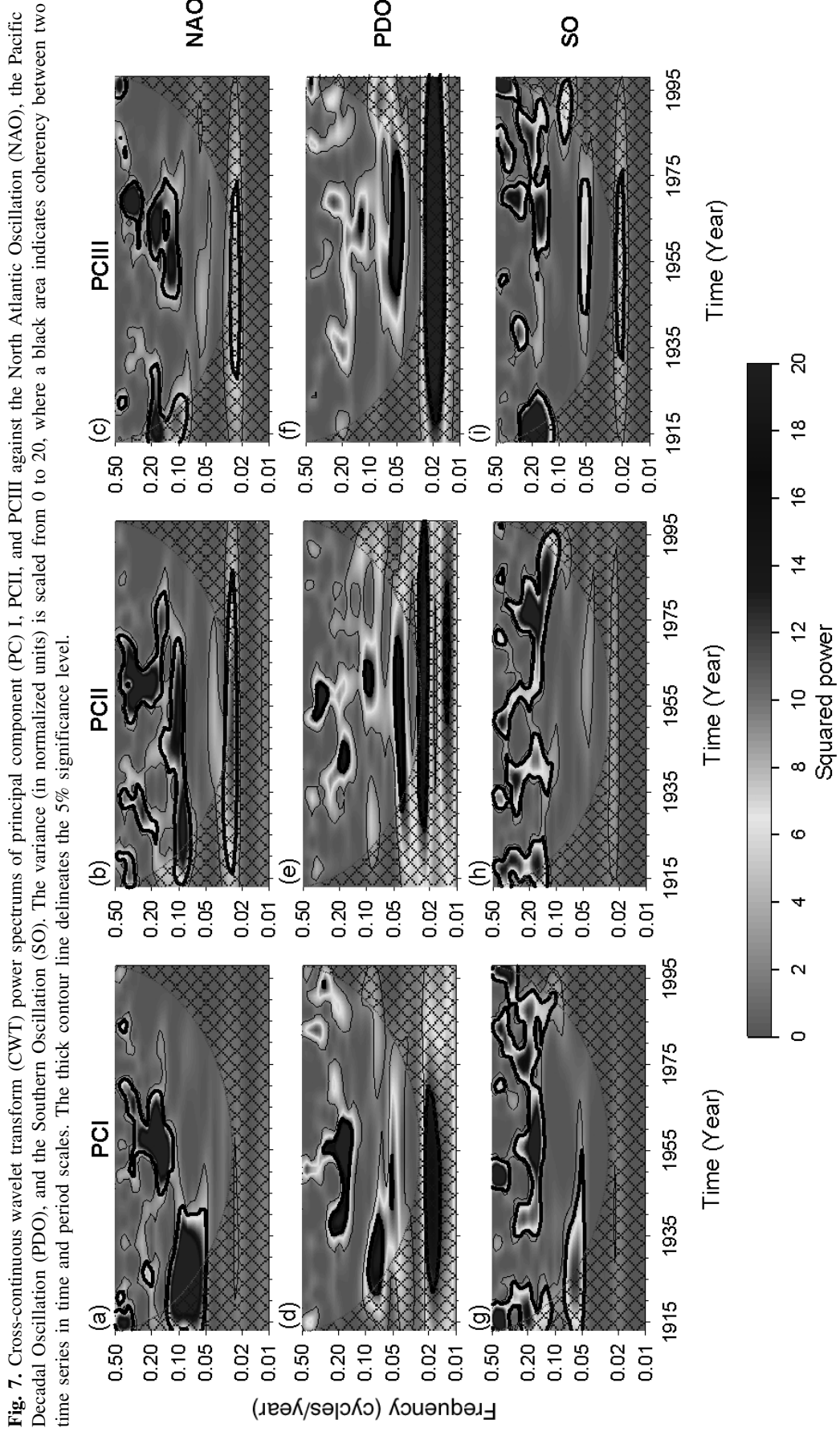
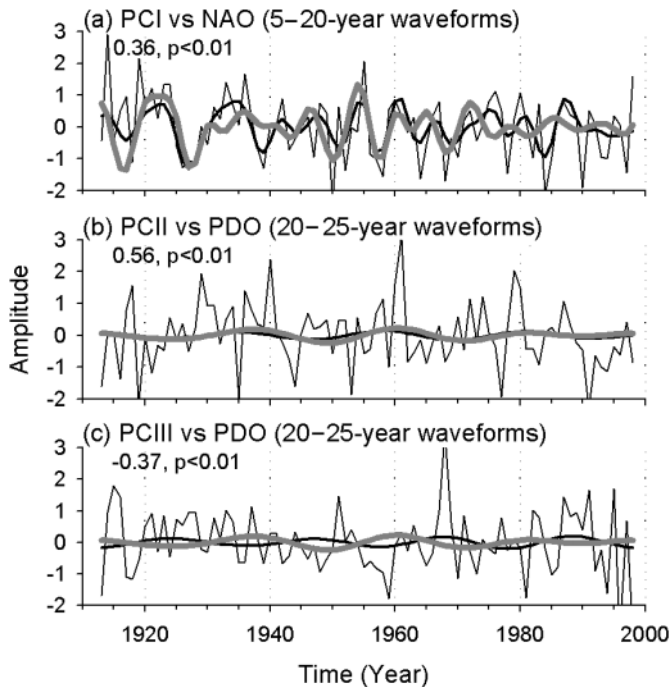


**Fig. 7.** Cross-continuous wavelet transform (CWT) power spectra of principal component (PC) I, PCII, and PCIII against the North Atlantic Oscillation (NAO), the Pacific Decadal Oscillation (PDO), and the Southern Oscillation (SO). The variance (in normalized units) is scaled from 0 to 20, where a black area indicates coherency between two time series in time and period scales. The thick contour line delineates the 5% significance level.

**Fig. 8.** Examples of coherencies among principal component (PC) analysis loadings (thin lines) and atmospheric circulation pattern indices. In (a) are shown 5- to 20-year waveforms. In (b) and (c) are shown 20- to 25-year waveforms. Waveforms associated with the PCs are shown as thick, black, smoothed lines. Waveforms associated with the circulation indices appear as thick, grey lines. The Kendall's rank correlation coefficient (with  $p$  value) is given for each pair of waveforms. NAO, North Atlantic Oscillation; PDO, Pacific Decadal Oscillation.



### Synoptic climatology

Our eigenvectors analysis suggests that the dominant mode of atmospheric circulation over the corridor resembles a strong zonal flow (latitudinal winds) accompanied by a weak meridional component that develops in July (longitudinal winds). The persistence of the high-pressure anomalies either over or upstream of the affected sector contributes to the development of the meridional flow. Bonsal et al. (1999) and Skinner et al. (1999) suggest that under these conditions, a northward and southward deflection of the moisture-carrying systems occurs. The subsistence of air (warming and drying) associated with the positive anomalies contributes to the development of a water deficit, given the absence of precipitation and increase in surface evaporation (Skinner et al. 1999). This mechanism is conducive to the occurrence of severe drought seasons and large seasonal area burned (Skinner et al. 1999).

Causes for interannual and interdecadal variations in drought severity have been briefly investigated, with the composites and the coherency analyses conducted on dominant atmospheric circulation patterns. Although it is recognised that these are mostly winter circulation patterns, several investigations have concluded that they are strong enough during summer to affect regional climate (Bonsal et al. 1993; Bonsal and Lawford 1999; Skinner et al. 1999). Based on the cross-CWT analyses, the NAO has been active

in the summer period, particularly in the centre of the corridor. The coherency was stronger in the frequency band of 5–20 years/cycle, with a shift around the mid-century toward an increase in interannual forcing. The relationship appears to be decoupled since the 1970s. A response in lower frequencies (20–25 years/cycle) also appears to be emerging from the North Pacific. However, given the length of the data array and the limited number of wavelengths in the low frequency band, it is difficult to fully quantify the PDO response.

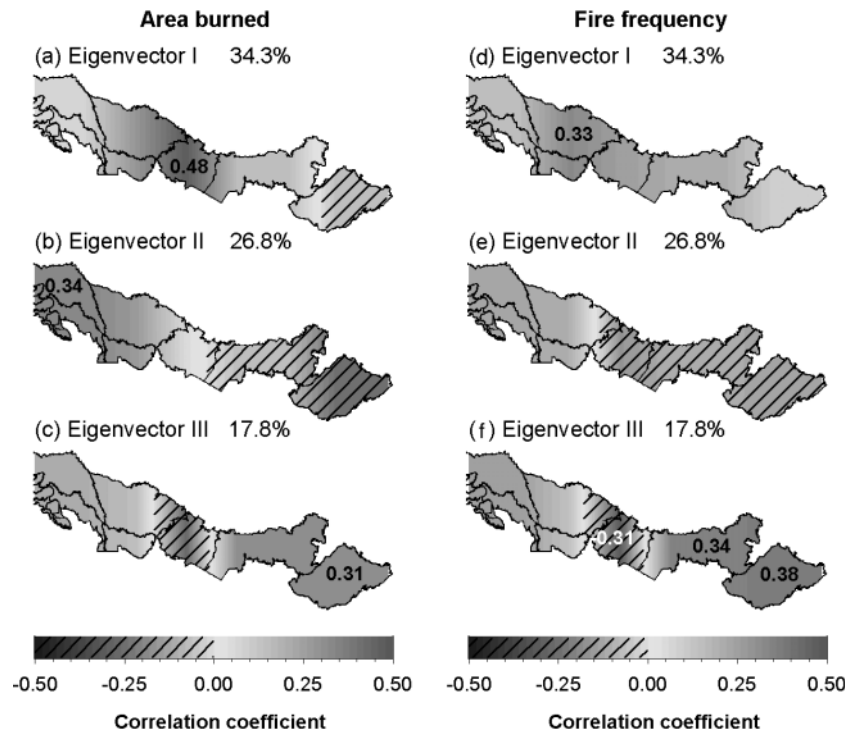
As pointed out by Yarnal et al. (2001), several studies have documented the instability of the atmosphere–surface relationships and further raised serious questions about the long-term reliability of climate prediction models (such as general circulation models). Circulation patterns are dynamic, and wide variations in their amplitude and periodicities occurred over the last 3 centuries (Stahle et al. 1998; Luterbacher et al. 2002; D'Arrigo et al. 2001; Girardin et al. 2002). Trying to determine the true relationships between the oceans and the atmosphere is also a great challenge, given the numerous inconsistencies among authors who attempted the task (Mehta et al. 2000; Robertson et al. 2000; Seager et al. 2000). This may be complicated by the non-stationarity and nonlinearity of the ocean atmosphere couplings, but also by the length of the instrumental time series, which seriously limits the interpretation of the low frequency signals. A comprehensive study of the multicentury climate change based on proxy data may be a prerequisite for the understanding of the present and prediction of the future climates.

### Limitation of the CDC

The CDC is a meteorological estimate, not an absolute drought index (Turner 1972). By using the Thornthwaite and Mather (1955) potential evapotranspiration models, the CDC calculation makes no allowance for seasonal changes in vegetation but only in daylight length (see Turner 1972). Temporal vegetation changes affect the water balance, as the development of herbs and shrubs tends to preserve ground moisture (Hély et al. 2000). This effect may, however, be counteracted by the development of the foliage, which contributes to increasing plant transpiration. In addition, the amount of precipitation (eq. 2) allocated for canopy interception in the CDC calculation procedure is arbitrary and may vary from one stand type to another, reflecting changes in vegetation. Other potential evapotranspiration estimation problems may be encountered because soil type, drainage, slope, watershed, atmospheric turbidity, cloudiness, changes in atmospheric  $\text{CO}_2$ , as well as many other meteorological, geological, and ecological parameters that can affect soil moisture content are not accounted for.

Other uncertainties within the CDC indices arise from exceptionally dry springs caused by an insufficient amount of snow. It is recognised that weather stations in Canada generally receive enough winter precipitation to saturate the CDC layer at spring (Turner and Lawson 1978; Alexander 1982). Exceptional years may, however, occur in regions west of Lake Nipigon and in the Great Plains. As the monthly lagged correlation between CDC indices decreases importantly from May to July (drought variability in May non-correlated with that of July), this limitation may be of minor

**Fig. 9.** Correlations maps demonstrating the relationship between drought severity and area burned (*a, b, c*) and fire frequency (*d, e, f*) (period 1959–1998). The eigenvectors I, II, and III denote the correlation between the principal components (computed from the July mean monthly average Canadian Drought Code (CDC) indices) and the fire statistics. Correlations are significant at  $p < 0.05$  when  $-0.31 > r > 0.31$  (significant correlation coefficients are shown on maps). For each map, the percentage of explained variance is indicated.



importance in the investigation of summer drought variability within our corridor. Studies to be conducted elsewhere could necessitate adaptations to the CDC calculation.

## Summary

This paper summarizes the construction of a network of monthly average CDC indices using 62 meteorological stations distributed across the corridor extending from central Quebec to western Manitoba, in the range of the southern Canadian boreal forest. These records were used for the construction of regional CDC indices in six climatic regions. Linear trends fitted on the regional mean monthly averages revealed no major changes in summer drought severity from 1913 to 1998.

This paper also demonstrates the potential use of CDC indices in synoptic climatology. Composites and coherency analyses indicated that the North Atlantic and the North Pacific circulation patterns demonstrate the strongest relationship with the drought variance. The coherencies, however, occur in a decadal scale, and the CDC data length seriously limits our interpretation of the responses. Validation of these relationships may require the use of long paleoclimatic records. Combined with regional fire history studies developed from forest stand age distributions, paleoclimatic analyses may provide useful insights on the causes of the changes in eastern Canada's forest fire regime. Such understanding would benefit the prediction of the response of the boreal forest to the anticipated climate change.

## Acknowledgements

We acknowledge the Sustainable Forest Management Network (SFM) for funding this research and supporting M.P. Girardin. This author was also supported by the Fonds Québécois de la Recherche sur la Nature et les Technologies and by Groupe de recherche en écologie forestière inter-universitaire (GREFI), Université du Québec à Montréal. We thank Dr. Christopher Torrence, Dr. Richard Holmes, the National Oceanic and Atmospheric Administration (NOAA), the Cooperative Institute for Research in Environmental Sciences (CIRES), the Climate Diagnostics Center (CDC), the National Centers for Environmental Prediction (NCEP), the National Center for Atmospheric Research, and the Meteorological Service of Canada for their aid and contribution of data and (or) software. This manuscript was improved through the comments of Héroïse Le Goff, Dr. D. Maynard, and two anonymous reviewers.

## References

- AISN Software. 1999. AutoSignal, version 1.5 for Windows. SPSS Inc., Chicago, Ill.
- Alexander, M.E. 1982. Calculating spring Drought Code starting values in the Prairie Provinces and Northwest Territories. Environment Canada. Canadian Forest Service, Northern Forestry Centre, Edmonton, Alta. For. Manage. Note 12.
- Archambault, S., and Bergeron, Y. 1992. An 802-year tree-ring chronology from the Quebec boreal forest. *Can. J. For. Res.* **22**: 674–682.

- Barlow, M., Nigam, S., and Berbery, E.H. 2001. ENSO, Pacific decadal variability, and U.S. summertime precipitation, drought, and stream flow. *J. Clim.* **14**: 2105–2128.
- Barry, R.G., and Carleton, A.M. 2001. Synoptic and dynamic climatology. Routledge, New York.
- Bergeron, Y. 2000. Species and stand dynamics in the mixed woods of Quebec's boreal forest. *Ecology*, **81**: 1500–1516.
- Bergeron, Y., and Archambault, S. 1993. Decreasing frequency of forest fires in the southern boreal zone of Quebec and its relation to global warming since the end of the 'Little Ice Age'. *Holocene*, **3**: 255–259.
- Bergeron, Y., and Dubuc, M. 1989. Succession in the southern part of the Canadian boreal forest. *Vegetatio*, **79**: 51–63.
- Bergeron, Y., Gauthier, S., Kafka, V., Lefort, P., and Lesieur, D. 2001. Natural fire frequency for the eastern Canadian boreal forest: consequences for sustainable forestry. *Can. J. For. Res.* **31**: 384–391.
- Bergeron, Y., Denneker, B., Charron, D., and Girardin, M.P. 2002. Using dendrochronology to reconstruct disturbance and forest dynamics around Lake Duparquet, northwestern Quebec. *Dendrochronologia*, **20**: 175–189.
- Bonsal, B.R., and Lawford, R.G. 1999. Teleconnections between El Niño and La Niña events and summer extended dry spells on the Canadian Prairies. *International Journal of Climatology*, **19**: 1445–1458.
- Bonsal, B.R., Chakravarti, A.K., and Lawford, R.G. 1993. Teleconnections between North Pacific SST anomalies and growing season extended dry spells on the Canadian Prairies. *International Journal of Climatology*, **13**: 865–878.
- Bonsal, B.R., Zhang, X., and Hogg, W.D. 1999. Canadian Prairies growing season precipitation variability and associated atmospheric circulation. *Clim. Res.* **11**: 191–208.
- Carcaillet, C., Bergeron, Y., Richard, P., Fréchette, B., Gauthier, S., and Prairie, Y. 2001. Change of fire frequency in the eastern Canadian boreal forests: Does vegetation composition or climate trigger the fire regime? *J. Ecol.* **89**: 930–946.
- D'Arrigo, R., Villalba, R., and Wiles, G. 2001. Tree-ring estimates of Pacific decadal climate variability. *Climate Dynamics*, **18**: 219–224.
- Ecological Stratification Working Group. 1996. A national ecological framework for Canada. Agriculture and Agri-Food Canada and Environment Canada, Ottawa, Ont.
- Environment Canada. 2000. Canadian daily climate data: temperature and precipitation. Meteorological Service of Canada, Climate Monitoring and Data Interpretation Division of the Climate Research Branch, Downsview, Ont.
- Environment Canada 2002. Canadian Climate Normals 1971–2000. Canadian Climate Program, Environnement Canada, Atmospheric Environment Service, Downsview, Ont.
- Flannigan, M., and Harrington, J.B. 1988. A study of the relation of meteorology variables to monthly provincial area burned by wildfire in Canada 1953–1980. *J. Appl. Meteorol.* **27**: 441–452.
- Flannigan, M.D., and Wotton, B.M. 2001. Climate, weather, and area burned. *In Forest fires. Edited by E.A. Johnson and K. Miyanishi.* Academic Press Inc., New York. pp. 351–373.
- Flannigan, M.D., Cambell, I., Wotton, M., Carcaillet, C., Richard, P., and Bergeron, Y. 2001. Future fire in Canada's boreal forest: paleoecology results and general circulation model – regional climate model simulations. *Can. J. For. Res.* **31**: 854–864.
- Girardin, M.P., Tardif, J., and Bergeron, Y. 2001. Radial growth analysis of *Larix laricina* from the Lake Duparquet area, Quebec, in relation to climate and larch sawfly outbreaks. *Ecoscience*, **8**: 127–138.
- Girardin, M.P., Tardif, J., Flannigan, M.D., and Bergeron, Y. 2002. Multicentury reconstruction of the Canadian Drought Code, eastern Canada, and its relationships with atmospheric circulation. *In Abstracts for the 6th International Conference on Dendrochronology — Dendrochronology, Environmental Change and Human History, Université Laval, Québec, Que., 22–27 August 2002. Edited by M. Lindholm et al.* Université Laval, Québec. pp. 119–121.
- Girardin, M.P., Tardif, J., Flannigan, M.D., and Bergeron, Y. In press. Multicentury reconstruction of the Canadian Drought Code from eastern Canada and its relationships with paleoclimatic indices of atmospheric circulation. *Climate Dynamics*.
- Hély, C., Bergeron, Y., and Flannigan, M.D. 2000. Effects of stand composition on fire hazard in the mixedwood Canadian boreal forest. *J. Veg. Sci.* **11**: 813–824.
- Holmes, R.L. 1999. Dendrochronology program library and the dendroecology program library. Laboratory of Tree-Ring Research, University of Arizona, Tucson, Ariz.
- Houghton, J.T., Ding, Y., Griggs, D.J., Noguier, M., Van der Linden, P.J., Xiaosu, D., Maskell, K., and Johnson, C.A. 2001. Climate change 2001: the scientific basis. Contribution of Working Group I to the third assessment report of the Intergovernmental Panel on Climate Change (IPCC). Cambridge University Press, Cambridge, U.K.
- Hurrell, J.W. 1995. Decadal trends in the North Atlantic Oscillation regional temperatures and precipitation. *Science (Washington, D.C.)*, **269**: 676–679.
- Kalnay, E., Kanamitsu, M., Kistler, R., Collins, W., Deaven, D., Gandin, L., Iredell, M., Saha, S., White, G., Woollen, J., Zhu, Y., Chelliah, M., Ebisuzaki, W., Higgins, W., Janowiak, J., Mo, K.C., Ropelewski, C., Wang, J., Leetmaa, A., Reynolds, R., Jenne, R., and Joseph, D. 1996. The NCEP/NCAR reanalysis 40-year project. *Bull. Am. Meteorol. Soc.* **77**: 437–471.
- Lau, K.M., and Weng, H.Y. 1995. Climate signal detection using wavelet transform: how to make a time series sing. *Bull. Am. Meteorol. Soc.* **76**: 2391–2402.
- Lefort, P., Gauthier, S., and Bergeron, Y. 2003. The influence of fire weather and land use on the fire regime of the Lake Abitibi area, eastern Canada. *For. Sci.* **49**: 509–521.
- Legendre, P., and Legendre, L. 1998. Numerical ecology. Elsevier Science Inc., New York.
- Luterbacher, J., Xoplaki, E., Dietrich, D., Rickli, R., Jacobeit, J., Beck, C., Gyalistras, D., Schmutz, C., and Wanner, H. 2002. Reconstruction of sea level pressure fields over the Eastern North Atlantic and Europe back to 1500. *Climate Dynamics*, **18**: 545–561.
- Mantua, N.J., Hare, S.R., Zhang, Y., Wallace, J.M., and Francis, R.C. 1997. A Pacific decadal climate oscillation with impacts on salmon. *Bull. Am. Meteorol. Soc.* **78**: 1069–1079.
- Mehta, V.M., Suarez, M.J., Mangello, J., and Delwoth, T.L. 2000. Oceanic influence on the North Atlantic Oscillation and associated Northern Hemisphere climate variations. *Geophys. Res. Lett.* **27**: 121–124.
- Mekis, E., and Hogg, W.D. 1999. Rehabilitated and analysis of Canadian daily precipitation time series. *Atmos.–Ocean*, **37**: 53–85.
- Murphy, P.J., Mudd, J.P., Stocks, B.J., Kasischke, E.S., Barry, D., Alexander, M.E., and French, N.H.F. 2000. Historical fire records in the North American boreal forest. *In Fire, climate change, and carbon cycling in the boreal forest. Edited by E.S. Kasischke and B.J. Stocks.* Springer Publishing Company, New York. pp. 274–288.
- Nigam, S., Barlow, M., and Berbery, E.H. 1999. Analysis links Pacific decadal variability to drought and streamflow in the United States. *EOS*, **80**: 621–625.

- Robertson, B.W., Mechoso, C.R., and Kim, Y.-J. 2000. The influence of Atlantic sea surface temperature anomalies on the North Atlantic Oscillation. *J. Clim.* **13**: 122–138.
- Ropelewski, C.F., and Jones, P.D. 1987. An extension of the Tahiti-Darwin Southern Oscillation Index. *Mon. Weather Rev.* **115**: 2161–2165.
- Seager, R., Kushnir, Y., Visbeck, M., Naik, N., Miller, J.A., Krahnmann, G., and Cullen, H.M. 2000. Causes of Atlantic Ocean climate variability between 1958 and 1998. *J. Clim.* **13**: 2845–2862.
- Skinner, W.R., Stocks, B.J., Martell, D.L., Bonsal, B., and Shabbar, A. 1999. The association between circulation anomalies in the mid-troposphere and the area burned by wildland fire in Canada. *Theor. Appl. Clim.* **63**: 89–105.
- Stahle, D.W., D'Arrigo, R., Krusic, P.J., Cleaveland, M.K., Cook, E.R., Allan, R.J., Cole, J.E., Dunbar, R.B., Therrell, M.D., Gay, D.A., Moore, M.D., Stokes, M.A., Burns, B.T., Villanueva-Diaz, J., and Thompson, L.G. 1998. Experimental dendroclimatic reconstruction of the Southern Oscillation. *Bull. Am. Meteorol. Soc.* **79**: 2137–2152.
- Stocks, B.J., Mason, J.A., Todd, J.B., Bosch, E.M., Wotton, B.M., Amiro, B.D., Flannigan, M.D., Hirsch, K.G., Logan, K.A., Martell, D.L., and Skinner, W.R. 2003. Large forest fires in Canada, 1959–1997. *J. Geophys. Res. (D Atmos.)* **108**: no. D1, Jan. 2003.
- Tardif, J., and Bergeron, Y. 1997. Comparative dendroclimatic analysis of two black ash and two white cedar populations from contrasting sites in the Lake Duparquet region, northwestern Quebec. *Can. J. For. Res.* **27**: 108–116.
- ter Braak, C.J.F., and Smilauer, P. 1998. Canoco reference manual and user's guide to Canoco for windows: software for canonical community ordination (version 4). Microcomputer Power, Ithaca, N.Y.
- Thorntwaite, C.W., and Mather, J.R. 1955. The water balance. *Publications in Climatology*, **8**: 1–86.
- Torrence, C., and Compo, G.P. 1998. A practical guide to wavelet analysis. *Bull. Am. Meteorol. Soc.* **79**: 61–78.
- Torrence, T., and Webster, P.J. 1998. Interdecadal changes in the ENSO-Monsoon System. *J. Clim.* **12**: 2679–2690.
- Turner, J.A. 1972. The drought code component of the Canadian Forest Fire Behaviour System. *Can. For. Serv. Publ.* 1316.
- Turner, J.A., and Lawson, B.D. 1978. Weather in the Canadian Forest Fire Danger Rating system: a user guide to national standards and practices. *Can. For. Serv. Publ.* 1316.
- Van Wagner, C.E. 1974. Effect of duff weight on drying rate. *Can. For. Serv. Bi-Mon. Res. Notes*, **30**: 11–12.
- Van Wagner, C.E. 1987. Development and structure of the Canadian Forest Fire Weather Index System. *Can. For. Serv. For. Tech. Rep.* 35.
- Vincent, L.A., and Gullett, D.W. 1999. Canadian historical and homogeneous temperature datasets for climate change analyses. *International Journal of Climatology*, **19**: 1375–1388.
- Yarnal, B. 1993. *Synoptic climatology in environmental analysis: a primer*. Belhaven Press, London, U.K.
- Yarnal, B., Comrie, A.C., Frakes, B., and Brown, D.P. 2001. Development and prospects in synoptic climatology. *International Journal of Climatology*, **21**: 1923–1950.
- Zhang, X., Vincent, L., Hogg, W.D., and Niitsoo, A. 2000. Temperature and precipitation trends in Canada during the 20th century. *Atmos.–Ocean*, **38**: 395–429.
- Zhang, X., Hogg, W.D., and Mekis, É. 2001. Spatial and temporal characteristics of heavy precipitation events over Canada. *J. Clim.* **14**: 1923–1936.

## Appendix A

### Calculation of the CDC residual rainfall

The amount of moisture from any specific rainfall that is absorbed in the CDC layer is given by the difference in moisture equivalent (RP) after ( $d$ ; current day) and before ( $d - 1$ ; previous day) rain.

$$[A1] \quad \Delta RP = RP_d - RP_{d-1} = [400 \exp(-CDC_d/400)] - [400 \exp(-CDC_{d-1}/400)]$$

where the constant 400 represents the maximum theoretical moisture content of the soil. Once the effect of the rainfall phase is known, water absorbed ( $W_a$ ; in mm) equals

$$[A2] \quad W_a = (\Delta RP_{25})/1000$$

where 25 and 1000 (both in  $\text{kg/m}^3$ ) represents the standard load and the weight of water per volume. The amount of residual rainfall (Drought Code Residual, DCR) is calculated from the total amount of rainfall (in mm,  $R_a$ ) minus the intercepted rainfall ( $R_i = 0.17P + 1.27$ ) and the absorbed water ( $W_a$ ). Thus

$$[A3] \quad DCR = R_a - R_i - W_a$$